

Self-synchronized reflection-mode acousto-optic imaging system utilizing nanosecond laser pulses

LUKASZ J. NOWAK* AND WIENDELT STEENBERGEN

Biomedical Photonic Imaging Group, Faculty of Science and Technology, University of Twente, Drienerlolaan 5, 7522 NB, Enschede, The Netherlands

**l.j.nowak@utwente.nl*

Abstract: We present an acousto-optic imaging system operating in reflection-mode and utilizing a pair of compact, triggerable lasers with 532 and 1064 nm wavelength and nanosecond pulse duration. The system maps the fluence rate distribution of light transmitted through optically scattering samples. The imaging is performed using an acousto-optic probe comprising an ultrasound linear array with attached optical fiber on one side and a camera on the other. The described hardware configuration images samples with access restricted to one side only and ensures mobility of the entire setup. The major challenge of the introduced approach is mitigating the effects of laser parameter instabilities and precise synchronization of ultrasound and laser pulses. We solved this issue by developing an electronic feedback circuit and a microcontroller-based synchronization and control system triggering the ultrasound scanner. Schematics and details regarding control algorithms are introduced. The imaging performance of the system is demonstrated on examples of results obtained for solid, acoustically-homogeneous and optically scattering phantoms with and without light absorbing inclusions present. Adjusting the size and location of the region of interest within the camera sensor matrix and the number of laser pulses illuminating every frame allows for significant improvements in terms of the achievable peak signal to noise ratio. We demonstrate that the developed synchronization algorithm and system play a crucial role in ensuring imaging quality and accuracy.

© 2021 Optica Publishing Group under the terms of the [Optica Open Access Publishing Agreement](#)

1. Introduction

Acousto-optic imaging (AOI) is a technique that enables to visualize fluence rate distribution of light transmitted through an optically-scattering medium. This is achieved by simultaneous illumination and insonification of an investigated sample with short laser and ultrasound (US) pulses. A propagating acoustic wave causes motion of optical scatterers and, in turn, modulation of light. By controlling the delay between light and US pulses emission, the location of overlapping insonified and illuminated interaction volume can be adjusted. Determining the ratio of intensities of the detected modulated to unmodulated light for various imaging coordinates allows to map the fluence rate distribution of light travelling from one to the other optode. [1]. Such information, under certain conditions [2,3], allows to conclude about the optical absorption distribution in the medium. In addition, under specific circumstances the results can be utilized for fluence correction of photoacoustic signals [4,5].

Non-invasive mapping of optical properties of opaque samples is of potential interest in, e.g., various biomedical applications. AOI could be particularly useful in investigating internal structure of many different tissue types, which are characterized with high scattering coefficient and relatively low optical absorption [6–8]. However, there are also some major challenges associated with this imaging modality, which prevent it from rapid adoption outside the laboratory environment. This concerns primarily issues related to detection of weak acousto-optic signal

and high susceptibility to various ambient noise sources. A number of different approaches to development of AOI systems is presented in review articles [9–11].

Almost all of the described detection schemes of ultrasonically modulated light require coherent light sources, with the coherence length of the order of at least centimeters [12]. Although possibility of detecting acousto-optic signal with incoherent light sources has also been demonstrated [13], the underlying modulation and detection mechanisms are much less effective [14], and thus hardly considered for practical implementation. The energy of transmitted light pulses determines the achievable signal to noise ratio for a given detection scheme, and sets requirements for the data acquisition time and system hardware complexity. Theoretical and experimental studies on utilizing nanosecond laser pulses for AOI were presented in the literature, showing feasibility of such an approach [15,16]. The described investigations were based on tandem pulses phase-locked with US signal, and required high-energy pulsed laser and relatively complex and large optical setups.

In the present study we focus on reflection-mode AOI, i.e., an arrangement in which US probe and the optodes are located on the same side of an investigated sample. Such an approach allows imaging of samples too thick for backlight illumination-detection or in cases when the region of interest is accessible from one side only. Various studies on reflectance geometry for AOI were presented by Lev et al. [17–19], Hisaka [20], Hisaka and Sakura [21], Hong-Bo et al. [22], and Kim et al. [23]. In all of these studies the scanning was performed by physically displacing either the probe components or the imaged sample. In our previous works we have demonstrated that imaging in such a configuration is also possible with static setup and purely electronic beam scanning [2,3].

Shaping acoustic pressure field distribution inside an investigated sample is an important aspect of any AOI system. Using focused US pulses allows to achieve high pressure amplitudes within small focal volumes. However, depending on the type of US probe used and adopted apodization patterns, residual pressure field components might in this case significantly contribute to light modulation, limiting the achievable imaging performance [24,25]. Utilizing plane-wave instead of focused US pulses allows to mitigate this phenomenon when using linear US arrays [24]. Laudereau et al. [26] and Bocoum et al. [27,28] demonstrated plane-wave AOI systems operating in transmission geometry, using multiple pulses emitted at different angles and dedicated image reconstruction algorithms. The obtained images allowed for clear distinction of light absorbing inclusions inside the investigated, opaque samples.

Here, we present a complete acousto-optic imaging setup operating in reflection-mode geometry and utilizing compact nanosecond-pulse lasers. The construction of the described system enables easy transportation and thus utilization outside purely laboratory environment. An integrated acousto-optic probe can be pressed directly against an investigated sample. This, in combination with electronic beam scanning, eliminates the necessity of using water tank or any other medium for coupling. An important challenge associated with the described setup was ensuring precise synchronization and possibility of delay adjustments between laser and US pulses. The benefits of compact size, nanosecond light pulse duration and high coherence length come at a cost of temperature instability of the used diode-pumped solid state lasers. The later feature causes the beam parameters to fluctuate when using variable triggering rate, as the laser cannot reach thermal equilibrium in such a case. We solved this issue by developing an electronic feedback control system and dedicated control algorithm with laser triggered at a constant frequency. The demonstrated AOI system is adjustable in terms of number of laser pulses emitted per single data point, light source wavelength, and size of detector sensor matrix. Such features, as it is demonstrated, allow to optimize the imaging performance in respect to the optical properties of an investigated sample.

2. System configuration and operation principles

2.1. Hardware setup

One of the main assumptions underlying the design process of the described acousto-optic system was ensuring compactness and mobility. The measurement setup should enable transportation without the need of any complex disassembly or readjustment procedures. This imposed significant restrictions especially on the optical part design, excluding e.g., bulky laser systems as light sources or complex optical paths arranged on a large optical table. Also, we assumed that the system should operate in reflection-mode geometry, for which access to an investigated sample from one side only is sufficient to perform measurements. The final and obvious requirement was to ensure satisfactory imaging quality – i.e., the obtained results should present clearly visible fluence rate distribution profiles of light transmitted through highly scattering samples.

A block diagram of the developed imaging system is presented in Fig. 1. It includes an integrated acousto-optic probe for transmission of light through a sample and emission of US pulses; an ultrasound scanner; a laser triggered from a signal generator; a PC computer for data acquisition and flow control; and an electronic synchronization and feedback control system. The system components communicate with each other via various electronic interfaces.

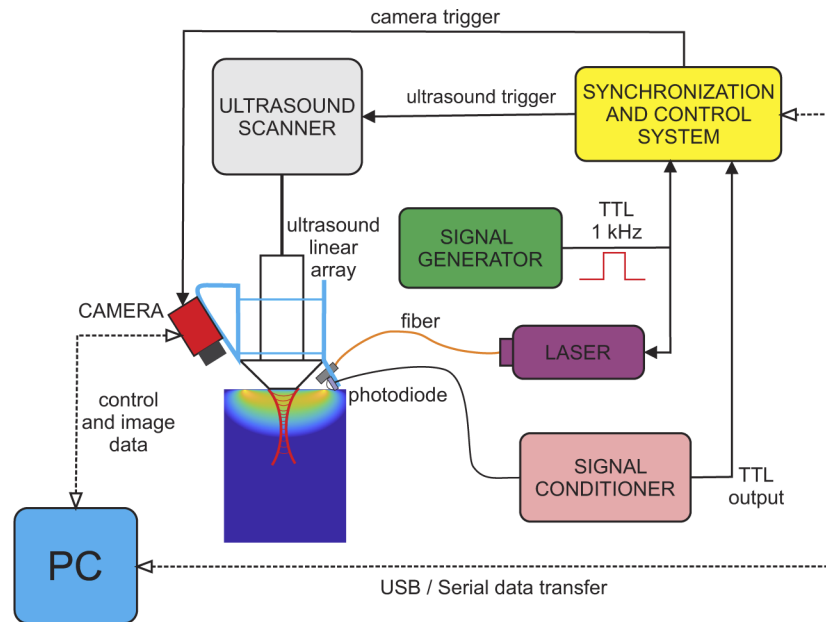


Fig. 1. The block diagram of the developed acousto-optic imaging system.

The system utilizes two pulsed lasers (Hübner photonics, Cobolt TOR XS models 0532-06-071-0050-0700 and 1064-06-071-0100-0700): one operating at 532 nm and the other at 1064 nm wavelength. The pulse energy is equal to, approximately, 50 μJ for 532 nm laser and 100 μJ for 1064 nm laser. The pulse duration is approximately 2,5 ns. The trigger to pulse jitter during steady state operation is declared to be less than 2 μs . We take advantage of these fluctuations by employing them in the detection scheme of acoustically modulated light. The lasers are operated one at a time, the unused device remains disconnected during measurements. The lasers have dimensions 40 mm x 40 mm x 80 mm, and are mounted on top of passive heatsinks. The corresponding power supplies are of the size and weight of a typical laptop computer power supply. The selected light sources are thus perfectly suitable to fulfill the adopted

design requirements regarding compactness and mobility. The lasers are triggered at a constant frequency of 1 kHz (the maximum supported frequency for the considered device types) with an external signal generator (Analog Discovery 2, Digilent). Both lasers with heatsinks are attached to an aluminum optical breadboard with dimensions 300 mm x 450 mm. In front of each of them a fiber coupler with a 3D-printed mounting system is attached. The laser pulses are coupled into 1000 μm diameter core multimode optical fibers (Thorlabs M35L01), which transmit the light directly to an integrated acousto-optic probe. The lasers and fiber coupling are presented in Fig. 2.

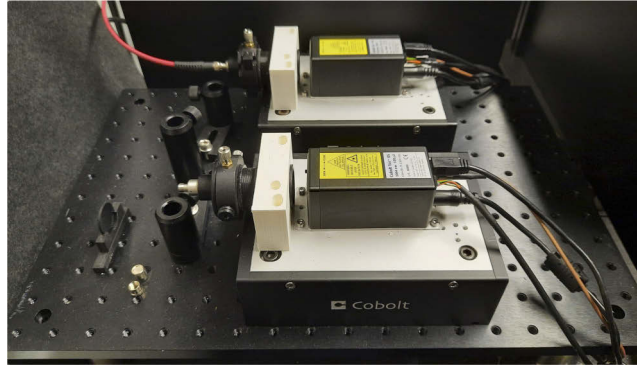


Fig. 2. A part of the optical setup: the lasers with fiber couplers.

The imaging probe is presented in Fig. 3. It includes a 128 element US linear array (ATL L7-4) operating at its center frequency of 5,208 MHz. The US transducer is enclosed in a custom-casted silicone grip, sandwiched between two aluminum plates. To the plates, on opposite sides of the transducer, 3D-printed fiber and camera holders are attached. Next to the fiber tip, a photodiode (BPW24R, Vishay) is also attached for detection of backscattered light, providing feedback information on the exact laser pulse emission moment. The CCD camera (Allied Vision ALVIUM 1800U-501NIR-CH-C) with objective lens (Computar M0824-MPW2) captures images of a sample surface adjacent directly to the US transducer. It is connected via USB to a PC computer, which performs initial device configuration and data acquisition.

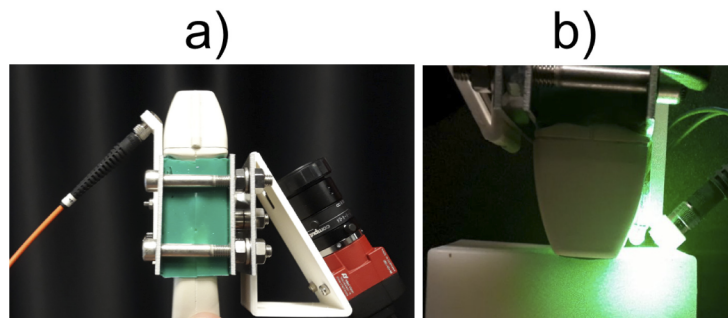


Fig. 3. An integrated acousto-optic probe: a) side view (without photodiode attached); b) during operation, on top of an optically scattering sample.

The US probe is connected to an ultrasound scanner (Verasonics Vantage 256). The scanner is triggered by an external electronic control system and excites US pulse emission accordingly to a programmed sequence. The specific settings for each sequence are generated using dedicated Matlab scripts. Here, we consider line scans along the probe axial direction performed using

plane wave US pulses. The pulses are generated by simultaneous excitation of all 128 transducer elements with 5 oscillation cycles.

2.2. Detection of modulated light

Photons transmitted through an optically scattering medium undergo multiple scattering events and take different propagation paths. If a coherent light source is used then, as a result of interference, the detected light will form a speckle pattern. A propagating acoustic wave causes optical scatterers to vibrate, and thus introduces fluctuations to the - otherwise steady - interference pattern. We use this information to determine the ratio of intensities of modulated to unmodulated light transmitted through an insonified volume [1].

For every single imaging point two subsequent camera frames are captured: first illuminated with a number of laser pulses, without US pulses present. And the second one, for which every laser pulse is accompanied with a synchronized US pulse. The delay between US and laser pulses is applied in such a way that the medium is illuminated when the US pulse has arrived at the desired location. For every captured camera frame a speckle contrast C value, given with the equation [29]:

$$C = \frac{\sigma}{\langle I \rangle}, \quad (1)$$

is calculated. σ denotes the standard deviation of the pixel values, and $\langle I \rangle$ is their mean value. By subtracting the results obtained for frames without and with US pulses present, speckle contrast difference (SCD) values for specified imaging coordinates (determined by the delay between US and laser pulses) are obtained.

The laser pulse duration in the described system is equal to approximately 2,5 ns. This value is much lower than the period of US pulses used for light modulation (approx. 192 ns). The corresponding movement of optical scatterers during a single period of illumination is thus negligible. For this reason the speckle patterns obtained using a single pulse frame illumination are not expected to reveal any significant contrast decrease. However, if more pulses are emitted during the camera exposure time, each of them will encounter the corresponding US pulse at slightly different moment. The primary source of such fluctuations is the laser's trigger to pulse jitter during steady state operation.

In order to increase signal to noise ratio, multiple frame pairs are acquired for every imaging point, and the calculated SCD values are averaged. The results presented in the present study were obtained for 30 frame pairs acquired for every data point.

2.3. Feedback control system and synchronization algorithm

Precise synchronization of laser and US pulses emission is crucial for imaging performance of the described system. In every case the acoustic wave needs to be illuminated at exactly specified moment of propagation, in order to be captured at desired imaging coordinates. Apart from US propagation delay, the synchronization algorithm has to take into account also the delay between the laser trigger and the actual pulse emission moment. The utilized light sources are passively Q-switched diode-pumped lasers, which require 200 - 250 μ s to build up after triggering. In the first approach, we triggered the lasers directly from the US scanner, assuming that the triggering delay is constant and equal to 250 μ s. However, it turned out that the shapes of the determined SCD plots as functions of imaging depths shift and change depending on the number of laser pulses used for illumination, wavelength, and demonstrate also time instability. Using photodiode and the signal conditioning circuit we determined the delay between moments of every laser pulse emission in a sequence and the associated triggering events. The results, presented in section 3, confirmed that the delay values fluctuate in time causing the described issues. We came to the conclusion that the source of the problem was variable triggering rate. The US scanner would perform the imaging sequence step by step, waiting for the data transfer from

the camera to finish after every single frame. This caused additional pauses between triggering events, which prevented the lasers from reaching thermal stability.

The solution to the instability issues described above is to let laser run constantly at a given triggering frequency. In such a case, after initial warm-up (approx. 15 minutes, as advised by the laser manual) the pump module reaches thermal equilibrium and the emission parameters are stable. Still, the exact delay time needs to be determined for every single measurement session, as it is device-specific and might also reveal long-term variability due to internal factors and ambient conditions. For this reason we developed a feedback control system providing information on the exact moment of laser pulse emission. The light is detected using a photodiode installed next to the fiber tip on an imaging probe, as shown in Fig. 3 b). The signal from the photodiode is however too weak to be directly fed to a microcontroller input port, and thus it requires additional conditioning. The photodiode output voltage needs to be converted into a TTL-level signal, while maintaining extremely short rise time (within tens of nanoseconds, to avoid significant readout distortions). We designed and constructed an electronic circuit fulfilling the adopted requirements, which performance was comprehensively evaluated experimentally. The schematic is presented in Fig. 4. The signal conditioning circuit met all the expectations for both 532 nm and 1064 nm laser pulses, without any noticeable errors during numerous measurement sessions.

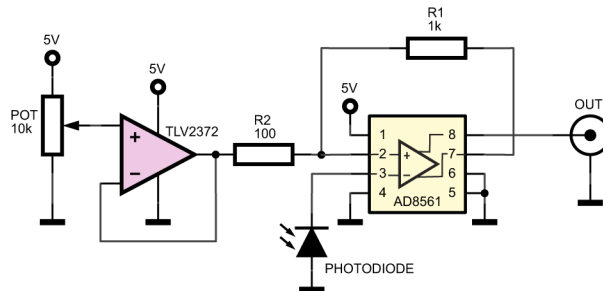


Fig. 4. A schematic of the photodiode signal conditioning circuit used to detect the exact moments of laser pulse emission.

Having the information on exact moment of laser pulse emission, it is possible to develop an algorithm and a control system which will utilize this data to synchronize operation of light source and the US scanner in the AOI system. As stated before, every imaging sequence consists of a number of camera frame pairs captured for specified imaging coordinates. The coordinates are determined by the delay between the emission of laser and US pulses. Since the laser to trigger delay is of the order of hundreds of μs , it is far greater than the expected propagation time of acoustic wave within a region of interest (between approximately 1 and 30 μs , depending on medium properties and assumed imaging depths). Thus, the laser needs to be triggered before the US transducer is excited, and the US scanner has to possess the knowledge on when exactly to expect the illumination to occur. This information is then utilized to perform the imaging sequence and delay US pulse emission accordingly to the programmed imaging coordinates.

The block diagram of the developed control algorithm is presented in Fig. 5. The algorithm was implemented on an ATmega328p microcontroller clocked with frequency of 16 MHz, using low level programming. The sequence begins with a "start" command, sent by a PC computer via serial port, followed by a number of laser pulses to be triggered within the current camera frame. Based on the external interrupt routines triggered by the signal generator driving laser and the photodiode signal conditioner output, the current delay between laser trigger and pulse emission is determined. Next, a value equivalent to 200 μs is subtracted from the determined delay, and the result is used as a count-down value for a timer. 200 μs is just an arbitrarily chosen value. It does not have any influence on the results as long as the remaining time (i.e.

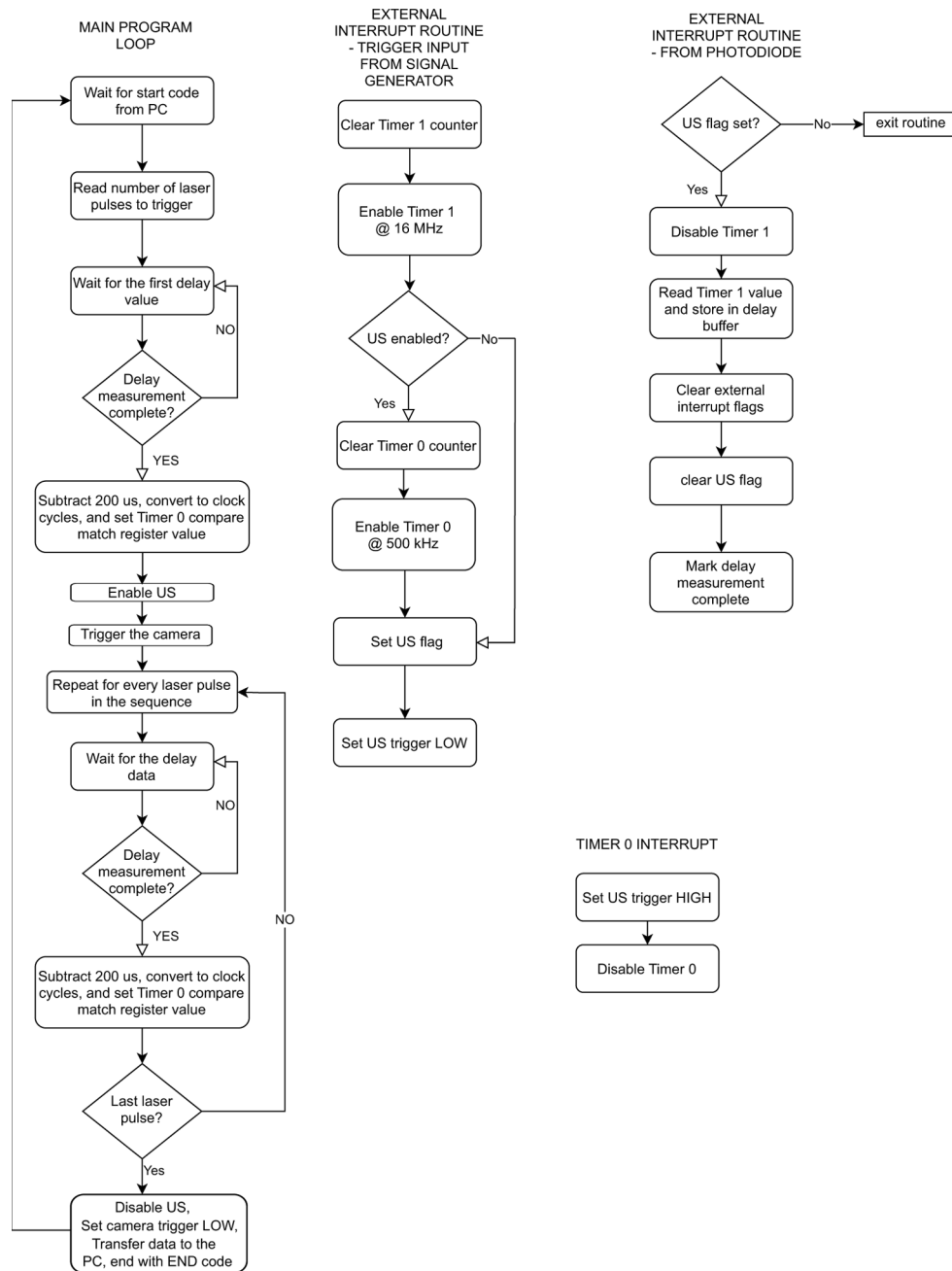


Fig. 5. A block diagram of the feedback control algorithm implemented on a microcontroller.

the laser to trigger delay minus the chosen value) is sufficient for the microcontroller to perform all the calculations. After the specified time the US scanner is triggered, expecting that the laser pulse emission will occur in exactly 200 μs . This allows to synchronize US and laser pulses and perform scanning in a pre-determined manner, while all the laser delay deviations are handled by the microcontroller. The camera is triggered directly before the first pulse in the sequence, and the described delay measurement and compensation routine is repeated for

every laser pulse illuminating the current frame. The camera exposure time is set by the PC computer before the measurement procedure starts, and it is equal to the given number of laser pulses in milliseconds (the laser trigger frequency is 1 kHz). After the sequence is finished, the microcontroller transfers the determined and stored delay values to the PC and acknowledges its readiness for the subsequent camera frame acquisition. A boolean variable "US flag" (Fig. 5) is used to emit US pulses only if the laser trigger was detected first.

A part of the control process is also operated by a PC computer connected in the system as presented in Fig. 1. The measurement procedure is programmed as a Matlab script. The PC initializes the camera and the microcontroller control system via USB ports, starts the data acquisition routine, and waits for the camera to transfer the image. Next, it calculates and stores the speckle contrast difference for the captured frame, and downloads the emission delay values of the corresponding laser pulses from the microcontroller. This routine is repeated for every single frame in the imaging sequence. After the last frame, the results are saved in a file, and the measurement procedure is stopped.

2.4. Measurement setup and procedures

In order to test the developed AOI system we conducted a number of experimental investigations on solid-state cuboid phantoms with dimensions of $70 \times 48 \times 35 \text{ mm}^3$. The phantoms were casted using polyvinyl chloride plastisol (PVCP, Lure Flex firm by Lure Factors) mixed with $3,5 \frac{\text{mg}}{\text{ml}}$ titanium dioxide (Sigma-Aldrich, particle size $44 \mu\text{m}$) for optical scattering. Three different phantoms were used in the measurements: one homogeneous, and two other with light absorbing inclusions. The inclusions were casted from the same material as the bodies of the phantoms, mixed additionally with ink, and injected into cylindrical through holes of diameter 3 mm. This allowed to keep the structures acoustically homogeneous, with propagation velocity determined to be $1700 \frac{\text{m}}{\text{s}}$. The inclusions were located centrally at various depths and oriented along the shortest edge – in parallel to the US linear array and centrally below it during the described measurements. One phantom had a single black inclusion 12 mm below the surface, and the other one had three inclusions: red, black and green located 10, 20, and 30 mm below the surface, respectively. Optical characteristics of the materials used for casting phantoms were determined using inverse adding-doubling method [30] applied to results of spectrophotometer measurements (Shimadzu UV-2600). The results are presented in Table 1.

Table 1. Determined optical properties of materials used for casting the phantoms

Reduced scattering coefficient μ'_s		
Dye	@532 nm	@1064 nm
No dye	$4,7 \text{ cm}^{-1}$	$1,3 \text{ cm}^{-1}$
Black	$3,1 \text{ cm}^{-1}$	N/A
Red	$10,7 \text{ cm}^{-1}$	$4,4 \text{ cm}^{-1}$
Green	$2,7 \text{ cm}^{-1}$	$0,5 \text{ cm}^{-1}$
Absorption coefficient μ_a		
Dye	@532 nm	@1064 nm
No dye	$\approx 0 \text{ cm}^{-1}$	$\approx 0 \text{ cm}^{-1}$
Black	$17,3 \text{ cm}^{-1}$	$12,5 \text{ cm}^{-1}$
Red	$2,8 \text{ cm}^{-1}$	$\approx 0 \text{ cm}^{-1}$
Green	$\approx 0 \text{ cm}^{-1}$	$\approx 0 \text{ cm}^{-1}$

During measurements the lights were switched off, as the ambient light illuminates the camera sensor, decreasing significantly the achievable signal to noise ratio. Before every experiment we

let the laser to run freely for approximately 15 minutes in order to reach the thermal equilibrium and stabilize the parameters. Unless otherwise stated, 532 nm laser was used. The camera region of interest (ROI) was 504 pixels long (in the direction parallel to the US linear array orientation) and 20 - 200 pixels wide (depending on the measurement), adjacent to the visible US probe surface.

3. Measurement results

As stated in Section 2, in the first approach, we triggered the lasers directly from US scanner, not using the external signal generator. The light pulses were emitted in a programmed sequence including acquiring data from camera, which resulted in a variable delay between the triggering events. Examples of the results obtained for the homogeneous phantom and different numbers of laser pulses illuminating every camera frame are presented in Fig. 6. In a homogeneous scattering medium the fluence rate of the detected light is expected to take a banana-shaped distribution between the optodes [31]. Thus, the visualized cross-sections should reveal a single global maximum for a constant imaging depth. Such maximum is indeed visible in the presented plots, however its location varies and depends on the number of laser pulses used.

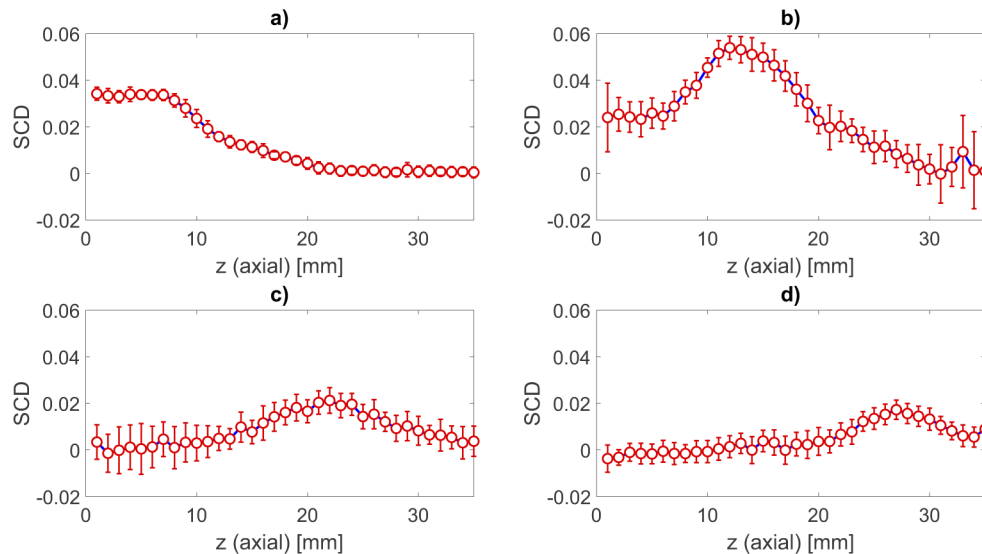


Fig. 6. Speckle contrast difference (SCD) values as functions of imaging depth obtained for a) 3, b) 5, c) 10, and d) 20 laser pulses per every camera frame, using variable laser triggering rate by the US scanner, assuming constant 250 μ s emission to trigger delay.

Figure 7 presents the laser pulse emission to trigger delays corresponding to the results from Fig. 6. The delay was not constant and equal 250 μ s as assumed, but varied for every pulse in an illumination sequence. There are also significant differences between pulse delays in first and last frames captured during every measurement. The mean values were determined by averaging over a total number of 2100 frames captured in each case (35 imaging points times 30 frame pairs). The fluctuations cause the laser pulses illuminate propagating acoustic waves not at the desired rendez-vous points, and thus explain the differences in plots presented in Fig. 6.

Figure 8 presents results analogous to the ones in Fig. 6, but obtained using the constant laser triggering frequency and the setup from Fig. 1. In such a case the SCD plots reveal distinct local maxima at identical imaging depths.

The laser pulse emission to trigger delays determined for the AOI setup presented in Fig. 1 revealed no significant fluctuations deteriorating image quality. A representative example of

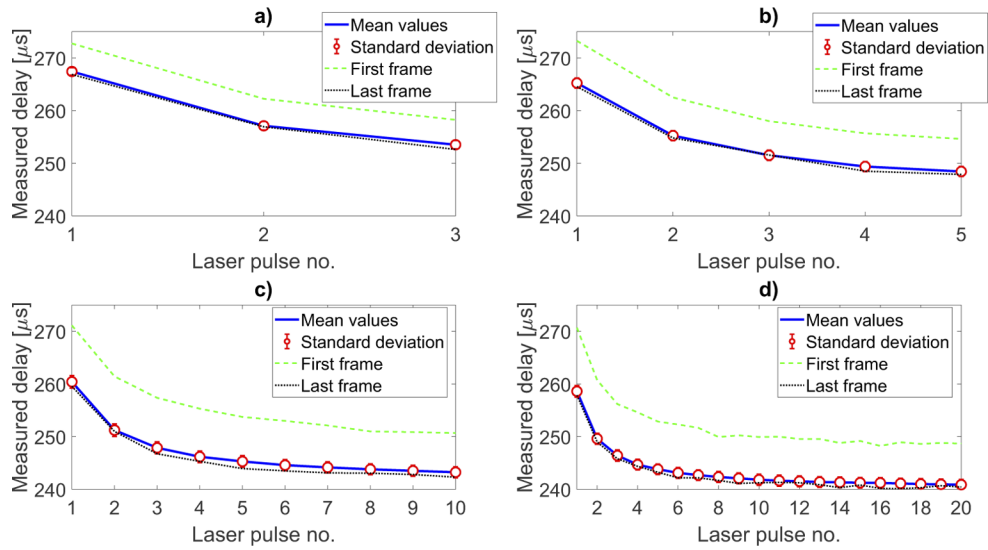


Fig. 7. Laser pulse emission to trigger delays determined for a) 3, b) 5, c) 10, and d) 20 laser pulses per every camera frame, using variable laser triggering rate by the US scanner (without external signal generator). Mean values and delays for first and last frame for every imaging sequence of 2100 frames are presented.

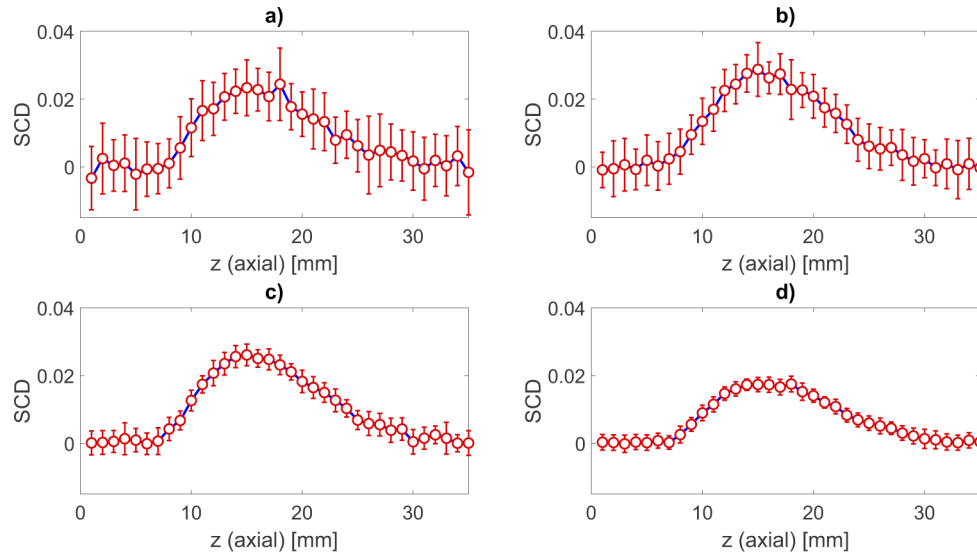


Fig. 8. Speckle contrast difference (SCD) values as functions of imaging depth obtained for a) 3, b) 5, c) 10, and d) 20 laser pulses per every camera frame, with laser triggered by an external signal generator at constant frequency of 1 kHz. Camera ROI width was set to 200 pixels.

results of delay measurements obtained for 20 pulses illuminating every camera frame and averaged over 2100 frames is presented in Fig. 9. The determined standard deviation of delay values was approximately 200 ns, which was typical for all the investigated cases. Such a deviation value corresponds to approximately 0.34 millimeter in acoustic propagation path within the considered media. The distributions of laser pulse to trigger delay values for both used

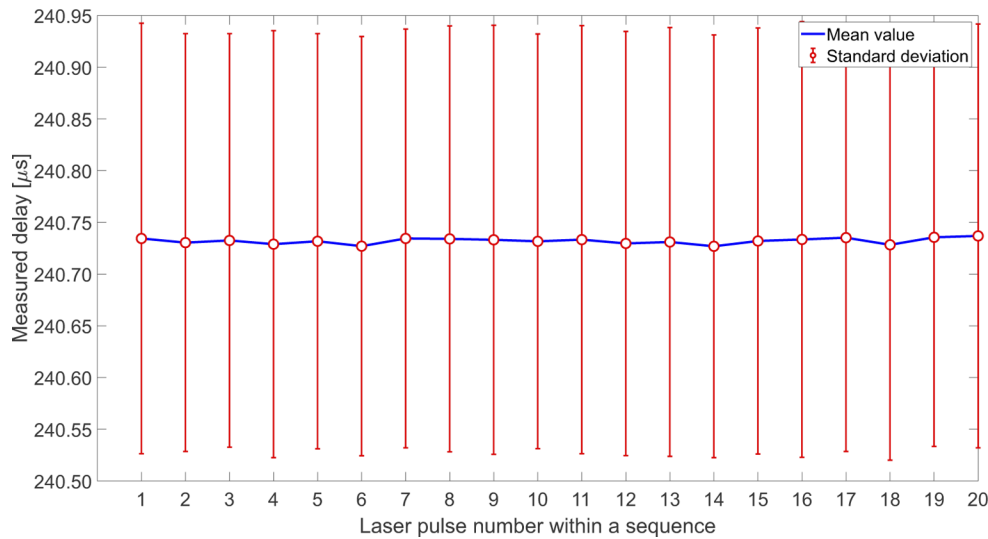


Fig. 9. Laser pulse emission to trigger delays determined for 20 laser pulses in an illumination sequence, averaged over 2100 captured camera frames.

lasers are presented in histograms in Fig. 10, plotted for 42000 pulses emitted within single imaging sequences (35 imaging points times 30 frame pairs per point times 20 pulses per frame). The delays did not exceed 2 μs maximum jitter value, declared in the documentation of the lasers. One should also notice that the determined values account for both actual laser delays and measurement system inaccuracies.

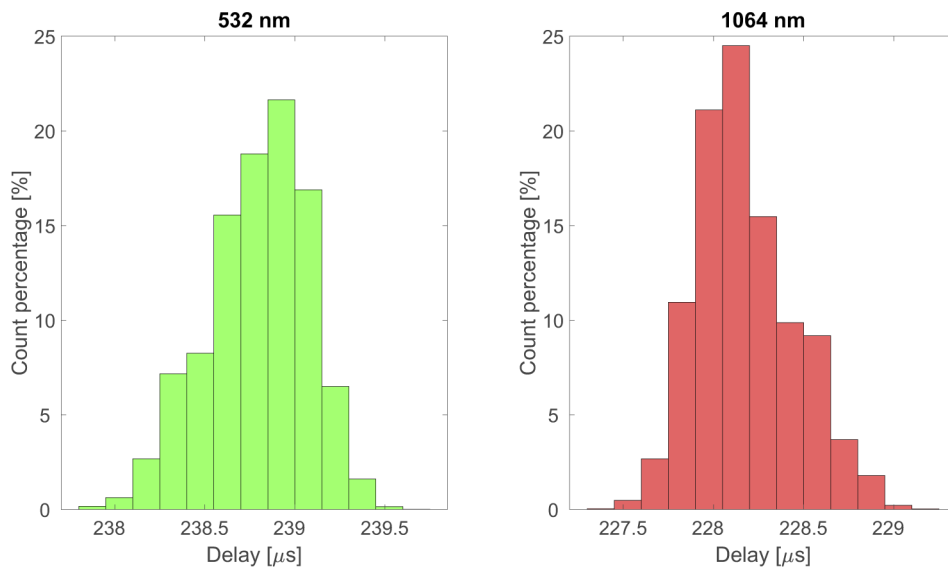


Fig. 10. Histograms presenting the determined laser pulse to trigger delay distributions for both 532 nm and 1064 nm lasers.

The fluctuations of laser trigger to pulse delays illustrated in Figs. 9 and 10 are greater than the US signal period (approx. 192 ns). The interference patterns resulting from adding up single illumination events will thus differ significantly, leading to contrast decrease compared to the

situation without light modulation by US pulses. This mechanism is illustrated with the example of speckle contrast difference plots obtained for one, two, and five laser pulses used to illuminate every single frame in the sequence, presented in Fig. 11. The values determined for the case of single pulse illumination fluctuate around zero, without any significant extrema. However, if two laser pulses are used for every frame, the expected profile with a single global maximum emerges. Adding more laser pulses improves signal to noise ratio and makes the maximum more distinct, at the very same position.

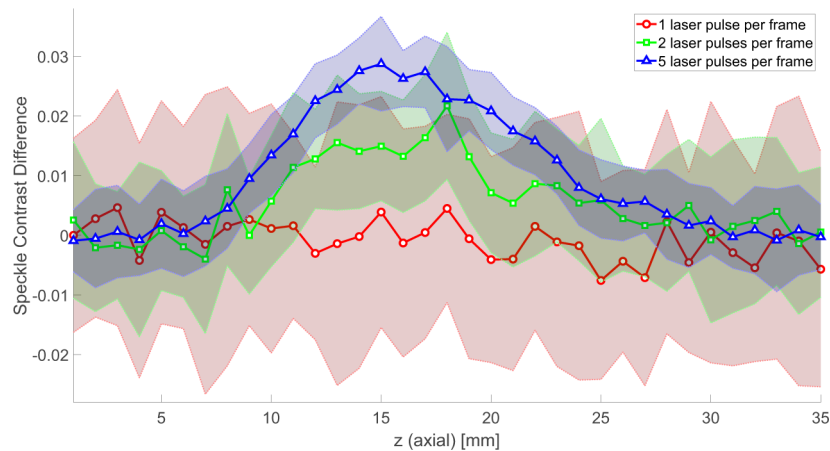


Fig. 11. Speckle contrast difference values as functions of imaging depth, obtained for the homogeneous phantom using different numbers of laser pulses in an illumination sequence and averaged over 30 frame pairs per point. The shaded areas indicate standard deviations. Camera ROI width was set to 200 pixels.

Figure 12 presents speckle contrast difference values obtained for two different phantoms: one without any absorbing inclusions, and the other with a single black inclusion 12 mm below the surface. The results were determined for both 532 nm and 1064 nm laser illumination, using 10 pulses per frame in each case. The camera ROI width was set to 50 pixels. Presence of the optically absorbing region causes significant decrease in the observed values. This is consistent with our previous findings on the relations between sample structures and reconstructed fluence rate distributions in reflection-mode AOI systems with electronically scanned US beam [2,24]. The achievable SCD values are significantly lower for 1064 nm wavelength, which might be related to large discrepancies in quantum efficiencies of the CCD camera (over 90 % at 532 nm vs. less than 5 % at 1064 nm). Still, the influence of the absorbing inclusion is clearly visible in both cases.

Figure 13 presents analogous results obtained for phantoms without any inclusions and with three inclusions: red, black, and green, located 10, 20 and 30 mm below the surface, respectively. The differences between plots are barely visible for 1064 nm laser illumination. For 532 nm laser there is a significant decrease in the determined SCD values, with a barely noticeable local minimum corresponding to the location of the black inclusion.

The camera in the developed system is a part of the integrated probe and looks directly at the surface of an investigated sample. Figure 14 presents examples of speckle patterns recorded using 5, 10, 15, and 20 laser pulses per frame for the homogeneous phantom. The average pixel intensities are not uniform across the introduced images, but vary along the y direction, perpendicular to the US transducer array orientation. It can be also seen in Fig. 14 d) that for 20 laser pulses per frame the pixels corresponding to the region closest to the US probe are clearly overexposed.

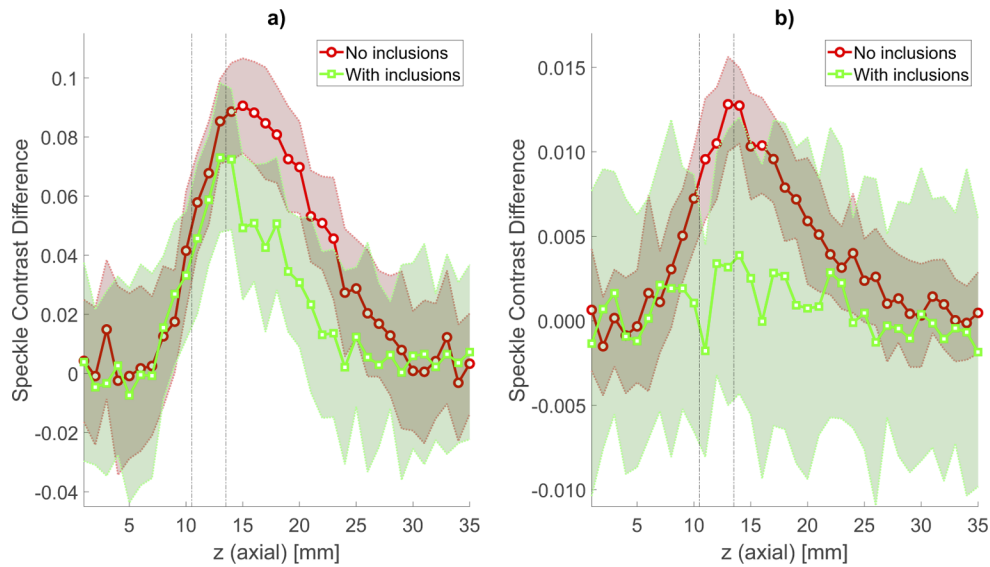


Fig. 12. Speckle contrast difference values as functions of imaging depth, obtained for phantoms without any inclusions and with a single black inclusion 12 mm below the surface, averaged over 30 frames per point: a) 532 nm laser illumination, b) 1064 nm laser illumination. The shaded areas indicate standard deviations, and the black, dashed lines indicate location of the inclusion. Camera ROI width was set to 50 pixels.

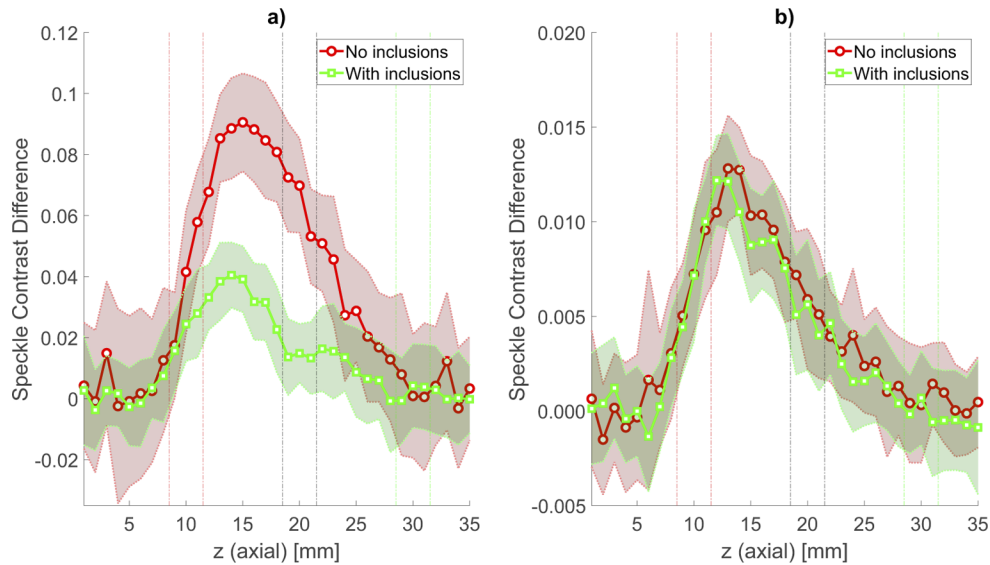


Fig. 13. Speckle contrast difference values as functions of imaging depth, obtained for phantoms without any inclusions and with three inclusions: red, black and green, located 10, 20 and 30 mm below the surface, respectively. a) 532 nm laser illumination, b) 1064 nm laser illumination. The shaded areas indicate standard deviations, and the dashed lines indicate locations of the inclusions. Camera ROI width was set to 50 pixels.

Comparison of the results presented in Figs. 8–13 shows that it is possible to adjust the laser pulse number and ROI width in order to optimize the system performance with respect to the

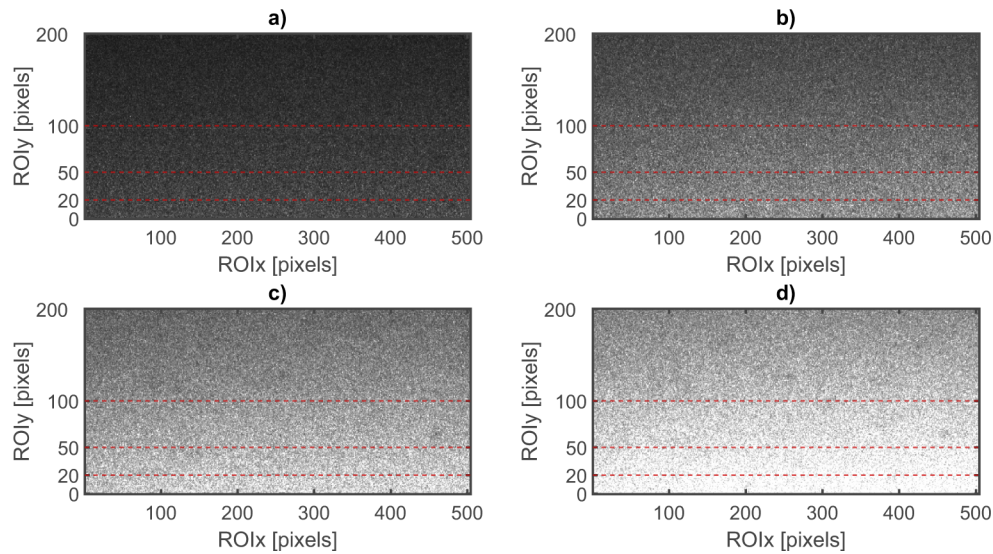


Fig. 14. Interference speckle patterns recorded by the camera using a) 5, b) 10, c) 15, and d) 20 laser pulses per frame for the homogeneous phantom.

maximum achievable SCD values. We determined peak SCD values for the homogeneous phantom, using different system settings. The results are presented in Fig. 15. Various ROI widths used for imaging are also indicated with red, dashed lines on speckle patterns in Fig. 14. The highest SCD values were achieved using 5 and 10 laser pulses per frame and ROI widths of 20 and 50 pixels. Increasing the number of pulses to 15 or more results in significant decrease in achievable contrast differences. The same is true for largest tested ROI width of 200 pixels.

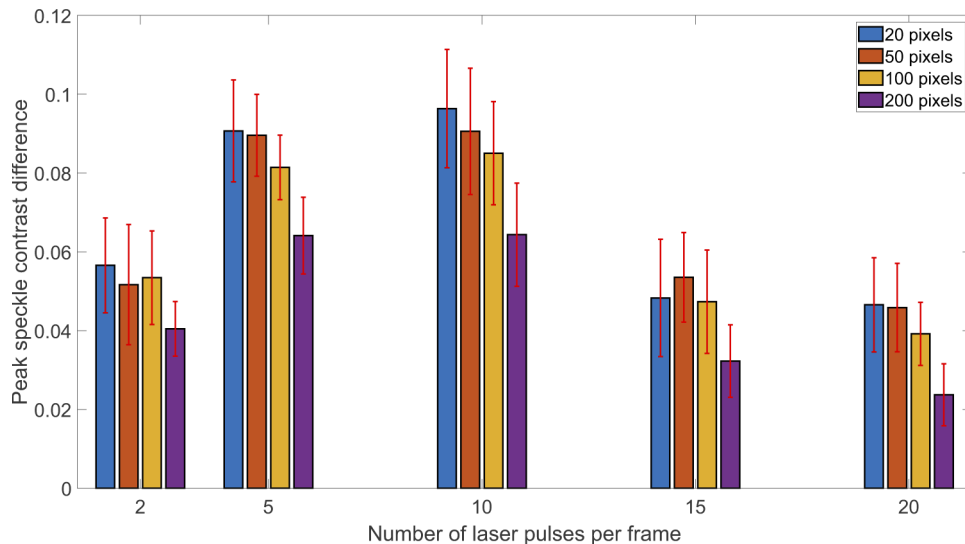


Fig. 15. Maximum achievable SCD values vs. number of laser pulses illuminating every frame determined using homogeneous phantom and different camera ROI widths. The error bars indicate standard deviation of the obtained peak values.

4. Discussion

The aim of the present study was to develop a reflection-mode acousto-optic imaging system suitable for use outside laboratory environment. The described measurement setup fulfills this condition, being easily transportable and not requiring any complex disassembly or re-adjustment procedures. The major challenge was to develop a self-contained optical part of the system, suitable to be used for AOI. We solved this problem by utilizing a pair of compact, nanosecond pulsed lasers mounted on a breadboard with custom made, 3d printed fiber couplers, control electronics and power supplies. The other AOI system components include US scanner (mounted on a cart), integrated acousto-optic probe, a PC computer with connected signal generator, and two small electronic circuits (photodiode signal conditioner and laser feedback control system). The whole setup can be easily disassembled/assembled by a single person in a relatively short time, and is ready for operation directly after connecting all the components together.

The most challenging part of the described system development was to ensure accurate synchronization between laser and US pulses. In the most direct approach, the lasers would be triggered directly by the US scanner in pre-determined moments within an imaging sequence. However, in such a case the US scanner would have to have a knowledge about exact delay between triggering events and laser pulse emission, and time span between trigger signals would be uneven. Such conditions turned out to be mutually exclusive due to the problems with reaching thermal stability by laser pumping stages. The examples of results presented in Figs. 6 and 7 clearly illustrate infeasibility of such a solution. Although the introduced design with external signal generator and electronic feedback control system is more complex than the described direct triggering scheme, it is indispensable to achieve any reasonable imaging performance in such a system. The examples of results presented in Figs. 8–9 confirm the validity of the adopted approach. It is worth emphasizing, that the developed control system and algorithm operate entirely autonomously, without the need of any manual adjustments or providing additional data before experiments. The adopted solution ensures that regardless of any long-term fluctuations of laser parameters due to, e.g., ambient temperature, aging, etc., the introduced AOI system will always be synchronized, performing accurately the programmed imaging sequence. Also, although both used lasers are characterized with significantly different triggering delay times (approximately 230 vs. 240 μ s), they can be simply switched between subsequent measurements, and the control system will immediately adjust.

As the laser is triggered with a constant frequency of 1 kHz, the number of pulses illuminating every acquired frame is equal to the set camera exposure time in milliseconds. Such a solution enables a direct manner to adjust system parameters. As illustrated in Fig. 11, at least two laser pulses are required in order to detect an acousto-optic signal. Increasing the number of pulses improves signal to noise ratio, but only to a certain level determined by the overexposure threshold. This can be clearly seen in the results presented in Figs. 14 and 15. The system can be adjusted in this regard for a specific medium to be investigated. The camera ROI size and location also determine the achievable SCD values. Due to the presence of intensity gradient resulting from the adopted light detection scheme, the pixels in the image closer to the US probe and transmitting fiber have higher values. This phenomenon is clearly seen in Fig. 14. Expanding ROI size over a certain level – as illustrated in Fig. 15 – causes low-intensity regions to be included, decreasing the overall signal to noise ratio and, thus, the achievable SCD values. The adjustment procedures are relatively simple and fast, and involve performing several test measurements for different ROI sizes and camera exposure time settings. All these changes are done in a single control script on the PC computer.

Presence of optically absorbing regions inside investigated samples may manifest itself in various ways in the reconstructed fluence rate distributions. The characteristics of the described system in this regard are in accordance with our previous findings regarding reflection-mode acousto-optic imaging with electronically scanned US pulses in general [2]. Primarily it will result

in decrease of detected SCD values. Under favorable conditions also local minima corresponding to the locations of the inclusions might be visible [2]. All these features are visible in the examples of results presented in Figs. 12 and 13. They also show that the sensitivity region of the system might extend to at least 20 mm in depth, however the imaging performance will always depend on the optical properties of the medium. Comparison of the data obtained for different laser wavelengths reveals significant variability in both shapes and levels of the SCD plots. Such differences constitute additional information on internal structures of the investigated samples.

The durations of the described imaging sequences ranged from approximately 70 s when using two laser pulses per frame, up to approximately 200 s when using 20 laser pulses illuminating every frame. The number of pulses determines the camera exposure time and thus achievable frame rate, and also the amount of data to be transferred between PC and the microcontroller via serial port after every single acquisition. In the considered examples 2100 frames were captured in each case (30 frame pairs for each of the 35 imaging points in a sequence). There are several possibilities to decrease the required imaging time. First, the number of frames per point can be reduced. This will decrease the signal to noise ratio, as less speckle contrast difference values will be available for averaging. The achievable improvements should be thus determined based on specific sample optical properties and acceptable output data quality. The same criteria might be used to determine the required number of laser pulses per frame. Another way to improve imaging time is to acquire less reference interference patterns for calculating speckle contrast difference values. In the presented examples every second camera frame was acquired without US pulses present, and the calculated speckle contrast value was used for subtraction of the analogous result obtained for the subsequent image. Such an approach makes the system more robust to parameter fluctuations. However, if the imaging time would be prioritized, the ratio of reference frames could be reduced resulting in proportional improvement in imaging speed.

The functionality of the developed AOI system can be extended with different imaging modalities. The developed hardware setup can be used without any modifications for both photoacoustic and ultrasound imaging. The laser pulse energy in our system is equal to 50 or 100 μJ (depending on the wavelength), which is comparable to the pulse energy used in some photoacoustic imaging systems [32]. The only required changes involve re-programming of the US scanner and the PC. Combination of AOI data with results of photoacoustic and US measurements can provide important information for, e.g., various biomedical applications by contributing to fluence correction [4,5]. Such a feature, along with ease of use outside laboratory environment, makes the system more versatile and expands the group of its potential users.

5. Conclusion

We developed a self-synchronized acousto-optic imaging (AOI) system, operating in reflection mode and utilizing plane wave ultrasound (US) pulses. The system can be transported and used outside laboratory environment without any complex re-assembly or re-adjustment procedures. This is possible primarily thanks to the use of a pair of compact nanosecond pulsed lasers with custom-made fiber couplers. We showed that in the described application the lasers have to be triggered with constant frequency in order to achieve thermal equilibrium and parameter stability. This imposes the major challenge of precise synchronization of US pulses with the moments of light emission. We solved this issue by developing a dedicated control algorithm and an electronic feedback control system. We demonstrated that using the developed AOI system it is possible to obtain information on optical properties of the investigated samples.

Funding. Nederlandse Organisatie voor Wetenschappelijk Onderzoek (15228).

Disclosures. The authors declare no conflicts of interest.

Data availability. Data underlying the results presented in this paper are not publicly available at this time but may be obtained from the authors upon reasonable request.

References

1. J. Li, G. Ku, and L. V. Wang, "Ultrasound-modulated optical tomography of biological tissue by use of contrast of laser speckles," *Appl. Opt.* **41**(28), 6030 (2002).
2. L. J. Nowak and W. Steenbergen, "Reflection-mode acousto-optic imaging using a one-dimensional ultrasound array with electronically scanned focus," *J. Biomed. Opt.* **25**(9), 096002 (2020).
3. L. J. Nowak and W. Steenbergen, "Reflection mode acousto-optic imaging using a 1-D ultrasound array," *Proc. SPIE* **11240**, 112402O (2020).
4. K. Daoudi, A. Hussain, E. Hondebrink, and W. Steenbergen, "Correcting photoacoustic signals for fluence variations using acousto-optic modulation," *Opt. Express* **20**(13), 14117–14129 (2012).
5. A. Hussain, E. Hondebrink, J. Staley, and W. Steenbergen, "Photoacoustic and acousto-optic tomography for quantitative and functional imaging," *Optica* **5**(12), 1579–1589 (2018).
6. S. L. Jacques, "Optical properties of biological tissues: a review," *Phys. Med. Biol.* **58**(11), R37–R61 (2013).
7. W. Cheong, S. Prahl, and A. Welch, "A review of the optical properties of biological tissues," *IEEE J. Quantum Electron.* **26**(12), 2166–2185 (1990).
8. J. L. Sandell and T. C. Zhu, "A review of in-vivo optical properties of human tissues and its impact on PDT," *J. Biophotonics* **4**(11-12), 773–787 (2011).
9. J. Gunther and S. Andersson-Engels, "Review of current methods of acousto-optical tomography for biomedical applications," *Front. Optoelectron.* **10**(3), 211–238 (2017).
10. D. S. Elson, L. Rui, D. Christopher, E. Robert, and T. Meng-Xing, "Ultrasound-mediated optical tomography: a review of current methods," *Interface Focus* **1**(4), 632–648 (2011).
11. S. G. Resink, A. C. Boccara, and W. Steenbergen, "State-of-the art of acousto-optic sensing and imaging of turbid media," *J. Biomed. Opt.* **17**(4), 040901 (2012).
12. G. Yao and L. V. Wang, "Theoretical and experimental studies of ultrasound-modulated optical tomography in biological tissue," *Appl. Opt.* **39**(4), 659–664 (2000).
13. C. W. Jarrett, C. F. Caskey, and J. C. Gore, "Detection of a novel mechanism of acousto-optic modulation of incoherent light," *PLoS One* **9**(8), e104268 (2014).
14. L. V. Wang, "Mechanisms of ultrasonic modulation of multiply scattered coherent light: an analytic model," *Phys. Rev. Lett.* **87**(4), 043903 (2001).
15. S. Resink, E. Hondebrink, and W. Steenbergen, "Solving the speckle decorrelation challenge in acousto-optic sensing using tandem nanosecond pulses within the ultrasound period," *Opt. Lett.* **39**(22), 6486–6489 (2014).
16. S. G. Resink and W. Steenbergen, "Tandem-pulsed acousto-optics: an analytical framework of modulated high-contrast speckle patterns," *Phys. Med. Biol.* **60**(11), 4371–4382 (2015).
17. A. Lev and B. G. Sfez, "Direct, noninvasive detection of photon density in turbid media," *Opt. Lett.* **27**(7), 473–475 (2002).
18. A. Lev, Z. Kotler, and B. G. Sfez, "Ultrasound tagged light imaging in turbid media in a reflectance geometry," *Opt. Lett.* **25**(6), 378–380 (2000).
19. A. Lev and B. Sfez, "In vivo demonstration of the ultrasound-modulated light technique," *J. Opt. Soc. Am. A* **20**(12), 2347–2354 (2003).
20. M. Hisaka, "Ultrasound-modulated optical parallel speckle measurement with stroboscopic illumination in a coaxial reflection system," *Appl. Phys. Lett.* **88**(3), 033901 (2006).
21. M. Hisaka and Y. Sasakura, "Light scattering characteristics of biological tissues in coaxial ultrasound-modulated optical tomography," *Jpn. J. Appl. Phys.* **48**(6), 067002 (2009).
22. F. Hong-Bo, X. Da, Z. Ya-Guang, W. Yi, and C. Qun, "Ultrasound-modulated optical tomography in reflective and coaxial configuration," *Chin. Phys. Lett.* **20**(12), 2165–2168 (2003).
23. C. Kim, K. H. Song, K. I. Maslov, and L. V. Wang, "Ultrasound-modulated optical tomography in reflection mode with ring-shaped light illumination," *J. Biomed. Opt.* **14**(2), 024015 (2009).
24. L. J. Nowak and W. Steenbergen, "Plane wave acousto-optic imaging in reflection mode geometry," *Proc. SPIE* **11642**, 116424R (2021).
25. L. J. Nowak and W. Steenbergen, "Reflection-mode acousto-optic imaging using plane wave ultrasound pulses," *J. Biomed. Opt.* **26**(9), 096001 (2021).
26. J.-B. Laudereau, A. A. Grabar, M. Tanter, J.-L. Gennisson, and F. Ramaz, "Ultrafast acousto-optic imaging with ultrasonic plane waves," *Opt. Express* **24**(4), 3774–3789 (2016).
27. M. Bocoum, J.-L. Gennisson, J.-B. Laudereau, A. Louchet-Chauvet, J.-M. Tualle, and F. Ramaz, "Structured ultrasound-modulated optical tomography," *Appl. Opt.* **58**(8), 1933–1940 (2019).
28. M. Bocoum, J.-L. Gennisson, A. A. Grabar, F. Ramaz, and J.-M. Tualle, "Reconstruction of bi-dimensional images in Fourier-transform acousto-optic imaging," *Opt. Lett.* **45**(17), 4855–4858 (2020).
29. R. Zemp, S. Sakadžić, and L. V. Wang, "Stochastic explanation of speckle contrast detection in ultrasound-modulated optical tomography," *Phys. Rev. E* **73**(6), 061920 (2006).
30. S. Prahl, *Optical Property Measurements using the Inverse Adding-Doubling Program* (Oregon Medical Laser Center, St. Vincent Hospital, 1999).

31. S. C. Feng, F. Zeng, and B. Chance, "Monte Carlo simulations of photon migration path distributions in multiple scattering media," in *Photon Migration and Imaging in Random Media and Tissues*, vol. 1888 (International Society for Optics and Photonics, 1993), pp. 78–89.
32. H. Zhong, T. Duan, H. Lan, M. Zhou, and F. Gao, "Review of low-cost photoacoustic sensing and imaging based on laser diode and light-emitting diode," *Sensors* **18**(7), 2264 (2018).